

Building and Interpreting Deep Similarity Models

Oliver Eberle, Jochen Büttner, Florian Kräutli, Klaus-Robert Müller, Matteo Valleriani, Grégoire Montavon

Abstract—Many learning algorithms such as kernel machines, nearest neighbors, clustering, or anomaly detection, are based on the concept of ‘distance’ or ‘similarity’. Before similarities are used for training an actual machine learning model, we would like to verify that they are bound to meaningful patterns in the data. In this paper, we propose to make similarities interpretable by augmenting them with an *explanation* in terms of input features. We develop BiLRP, a scalable and theoretically founded method to systematically decompose similarity scores on pairs of input features. Our method can be expressed as a composition of LRP explanations, which were shown in previous works to scale to highly nonlinear functions. Through an extensive set of experiments, we demonstrate that BiLRP robustly explains complex similarity models, e.g. built on VGG-16 deep neural network features. Additionally, we apply our method to an open problem in digital humanities: detailed assessment of similarity between historical documents such as astronomical tables. Here again, BiLRP provides insight and brings verifiability into a highly engineered and problem-specific similarity model.

Index Terms—Similarity, layer-wise relevance propagation, deep neural networks, explainable machine learning, digital humanities.



1 INTRODUCTION

Building meaningful similarity models that incorporate prior knowledge about the data and the task is an important area of machine learning and information retrieval [1], [2]. Good similarity models are needed to find relevant items in databases [3], [4], [5]. Similarities (or kernels) are also the starting point of a large number of machine learning models including discriminative learning [6], [7], unsupervised learning [8], [9], [10], [11], and data embedding/visualization [12], [13], [14].

An important practical question is how to select the similarity model appropriately. Assembling a labeled dataset of similarities for validation can be difficult: The labeler would need to inspect meticulously multiple pairs of data points and come up with exact real-valued similarity scores. As an alternative, selecting a similarity model based on performance on some proxy task can be convenient (e.g. [15], [16], [17], [18]). In both cases, however, the selection procedure is exposed to a potential lack of representativity of the training data (cf. the ‘Clever Hans’ effect [19]).—In this paper, we aim for a more direct way to assess similarity models, and make use of explainable ML for that purpose.

Explainable ML [20], [21], [22] is a subfield of machine learning that focuses on making predictions interpretable to

- O. Eberle is with the Berlin Institute of Technology (TU Berlin), 10587 Berlin, Germany.
- J. Büttner is with the Max Planck Institute for the History of Science, 14159 Berlin, Germany.
- F. Kräutli is with the Max Planck Institute for the History of Science, 14159 Berlin, Germany.
- K.-R. Müller is with the Berlin Institute of Technology (TU Berlin), 10587 Berlin, Germany; the Department of Brain and Cognitive Engineering, Korea University, Seoul 136-713, Korea; and the Max Planck Institut für Informatik, 66123 Saarbrücken, Germany. E-mail: klaus-robert.mueller@tu-berlin.de.
- M. Valleriani is with the Max Planck Institute for the History of Science, 14159 Berlin, Germany.
- G. Montavon is with the Berlin Institute of Technology (TU Berlin), 10587 Berlin, Germany. E-mail: gregoire.montavon@tu-berlin.de.

(Corresponding Authors: Grégoire Montavon, Klaus-Robert Müller)

the human. By highlighting the input features (e.g. pixels or words) that are used for predicting, explainable ML allows to gain systematic understanding into the model decision structure. Numerous approaches have been proposed in the context of ML classifiers [23], [24], [25], [26].

In this paper, we bring explainable ML to similarity. We contribute a new method that systematically explains similarity models of the type:

$$y(\mathbf{x}, \mathbf{x}') = \langle \phi_L \circ \dots \circ \phi_1(\mathbf{x}), \phi_L \circ \dots \circ \phi_1(\mathbf{x}') \rangle,$$

e.g. dot products built on some hidden layer of a deep neural network. Our method is based on the insight that similarity models can be naturally decomposed on *pairs* of input features. Furthermore, this decomposition can be computed as a combination of multiple LRP explanations [24] (and potentially other successful explanation techniques). As a result, it inherits qualities such as broad applicability and scaling to highly nonlinear models. Our method, which we call ‘BiLRP’, is depicted at a high level in Fig. 1.

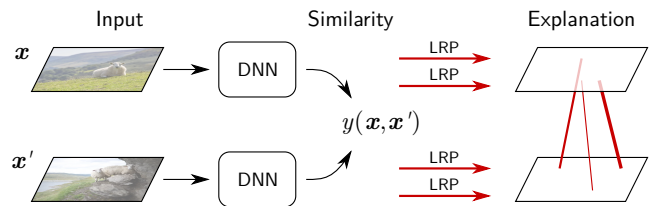


Fig. 1: Proposed BiLRP method for explaining similarity. Produced explanations are in terms of pairs of input features.

Conceptually, BiLRP performs a *second-order* ‘deep Taylor decomposition’ [27] of the similarity score, which lets us retrace, layer after layer, features that have jointly contributed to the similarity. Our method reduces for specific choices of parameters to a ‘Hessian \times Product’ baseline. With appropriate choices of parameters BiLRP significantly im-

proves over this baseline and produces explanations that robustly extend to complex deep neural network models.

We showcase BiLRP on similarity models built at various layers of the well-established VGG-16 image classification network [28]. Our explanation method brings useful insights into the strengths and limitations of each similarity model. We then move to an open problem in the digital humanities, where similarity between scanned astronomical tables needs to be assessed [29]. We build a highly engineered similarity model that is specialized for this task. Again BiLRP proves useful by being able to inspect the similarity model and validate it from limited data.

Altogether, the method we propose brings transparency into a key ingredient of machine learning: similarity. Our contribution paves the way for designing and validating similarity-based ML models in an efficient, fully informed, and human-interpretable manner.

1.1 Related Work

Methods such as LLE [30], diffusion maps [31], or t-SNE [14] give insight into the similarity structure of large datasets by embedding data points in a low-dimensional subspace where relevant similarities are preserved. While these methods provide useful visualization, their purpose is more to find *global* coordinates to comprehend a whole dataset, than to explain why two *individual* data points are predicted to be similar.

The question of explaining individual predictions has been extensively studied in the context of ML classifiers. Methods based on occlusions [32], [33], surrogate functions [25], [34], gradients [23], [35], [36], [37], or reverse propagation [24], [32], have been proposed, and are capable of highlighting the most relevant features. Some approaches have been extended to unsupervised models, e.g. anomaly detection [38], [39] and clustering [40]. Our work goes further along this direction and explains *similarity* by identifying relevant *pairs* of input features.

Several methods for joint features explanations have been proposed. Some of them extract feature interactions globally [41], [42]. Other methods produce individual explanations for simple pairwise matching models [43], or models with explicit multivariate structures [44]. Another method extracts joint feature explanations in nonlinear models by estimating the integral of the Hessian [45]. In comparison, our BiLRP method leverages the layered structure of the model to robustly explain complex similarities, e.g. built on deep neural networks.

A number of works improve similarity models by leveraging prior knowledge or ground truth labels. Proposed approaches include structured kernels [46], [1], [47], [48], or siamese/triplet networks [49], [50], [51], [52], [53]. Beyond similarity, applications such as collaborative filtering [54], transformation modeling [55], and information retrieval [56], also rely on building high-quality matching models between pairs of data.—Our work has an orthogonal objective: It assumes an already trained well-performing similarity model, and makes it explainable to enhance its verifiability and to extract novel insights from it.

2 TOWARDS EXPLAINING SIMILARITY

In this section, we present basic approaches to explain similarity models in terms of input features. We first discuss the case of a simple linear model, and then extend the concept to more general nonlinear cases.

2.1 From Linear to Nonlinear Models

Let us begin with a simple scenario where $\mathbf{x}, \mathbf{x}' \in \mathbb{R}^d$ and the similarity score is given by some dot product $y(\mathbf{x}, \mathbf{x}') = \langle W\mathbf{x}, W\mathbf{x}' \rangle$, with W a projection matrix of size $h \times d$. The similarity score can be easily decomposed on input features by rewriting the dot product as:

$$y(\mathbf{x}, \mathbf{x}') = \sum_{ii'} \langle W_{:,i}, W_{:,i'} \rangle \cdot x_i x'_{i'}. \quad (1)$$

We observe from Eq. (1) that the similarity is decomposable on *pairs* of features (i, i') of the two examples. In other words, input features interact to produce a high/low similarity score.

In practice, more accurate models of similarity can be obtained by relaxing the linearity constraint. Consider some similarity model $y(\mathbf{x}, \mathbf{x}') = \langle \phi(\mathbf{x}), \phi(\mathbf{x}') \rangle$ built on some abstract feature map $\phi: \mathbb{R}^d \rightarrow \mathbb{R}^h$ which we assume to be differentiable. A simple and general way of attributing the similarity score to the input features is to compute a Taylor expansion [24] at some reference point $(\tilde{\mathbf{x}}, \tilde{\mathbf{x}}')$:

$$\begin{aligned} y(\mathbf{x}, \mathbf{x}') &= y(\tilde{\mathbf{x}}, \tilde{\mathbf{x}}') \\ &+ \sum_i [\nabla y(\tilde{\mathbf{x}}, \tilde{\mathbf{x}}')]_i (x_i - \tilde{x}_i) \\ &+ \sum_{i'} [\nabla y(\tilde{\mathbf{x}}, \tilde{\mathbf{x}}')]_{i'} (x'_{i'} - \tilde{x}'_{i'}) \\ &+ \sum_{ii'} [\nabla^2 y(\tilde{\mathbf{x}}, \tilde{\mathbf{x}}')]_{ii'} (x_i - \tilde{x}_i) (x'_{i'} - \tilde{x}'_{i'}) \\ &+ \dots \end{aligned}$$

The explanation is then obtained by identifying the multiple terms of the expansion. Here again, like for the linear case, some of these terms can be attributed to pairs of features (i, i') . For general nonlinear models, it is difficult to systematically find reference points $(\tilde{\mathbf{x}}, \tilde{\mathbf{x}}')$ at which a Taylor expansion represents well the similarity score. To address this, we will need to apply some restrictions to the analyzed model.

2.2 The ‘Hessian \times Product’ Baseline

Consider the family of similarity models that can be represented as dot products on positively homogeneous feature maps, i.e.

$$\begin{aligned} y(\mathbf{x}, \mathbf{x}') &= \langle \phi(\mathbf{x}), \phi(\mathbf{x}') \rangle, \\ \phi: \mathbb{R}^d &\rightarrow \mathbb{R}^h \quad \text{with} \quad \forall_{\mathbf{x}} \forall_{t>0} : \phi(t\mathbf{x}) = t\phi(\mathbf{x}). \end{aligned}$$

The class of functions ϕ is broad enough to include (with minor restrictions) interesting models such as the mapping on some layer of a deep rectifier network [57], [28], [58].

We perform a Taylor expansion of the similarity function at the reference point $(\tilde{\mathbf{x}}, \tilde{\mathbf{x}}') = (\varepsilon\mathbf{x}, \varepsilon\mathbf{x}')$ with ε almost zero. Zero- and first-order terms of the expansion vanish, leaving us with a decomposition on the interaction terms:

$$y(\mathbf{x}, \mathbf{x}') = \sum_{ii'} [\nabla^2 y(\mathbf{x}, \mathbf{x}')]_{ii'} x_i x'_{i'} \quad (2)$$

(cf. Appendix A of the Supplement). Inspection of these interaction terms reveals that a pair of features (i, i') is found to be relevant if:

- (i) the features are jointly expressed in the data, and
- (ii) the similarity model jointly reacts to these features.

We call this method ‘Hessian \times Product’ (HP) and use it as a baseline in Section 4. This baseline can also be seen as a reduction of ‘Integrated Hessians’ [45] for the considered family of similarity models.

HP is closely connected to a common baseline method for explaining ML classifiers: Gradient \times Input [59], [60], [61]. The matrix of joint feature contributions found by HP can be obtained by performing $2 \times h$ ‘Gradient \times Input’ (GI) computations:

$$\text{HP}(y, \mathbf{x}, \mathbf{x}') = \sum_{m=1}^h \text{GI}(\phi_m, \mathbf{x}) \otimes \text{GI}(\phi_m, \mathbf{x}')$$

(cf. Appendix A.3 of the Supplement). This gradient-based formulation makes it easy to implement HP using neural network libraries with automatic differentiation. However, because of this close relation, ‘Hessian \times Product’ also inherits some weaknesses of ‘Gradient \times Input’, in particular, its high exposure to gradient noise [61]. In deep architectures, the gradient is subject to a shattering effect [62] making it increasingly large, high-varying, and uninformative, with every added layer.

3 BETTER EXPLANATIONS WITH BiLRP

Motivated by the limitations of the simple techniques presented in Section 2, we introduce our new BiLRP method for explaining similarities. The method is inspired by the ‘layer-wise relevance propagation’ (LRP) [24] method, which was first introduced for explaining deep neural network classifiers. LRP leverages the layered structure of the model to produce robust explanations.

BiLRP brings the robustness of LRP to the task of explaining dot product similarities. Our method assumes as a starting point a layered similarity model:

$$y(\mathbf{x}, \mathbf{x}') = \langle \phi_L \circ \dots \circ \phi_1(\mathbf{x}), \phi_L \circ \dots \circ \phi_1(\mathbf{x}') \rangle,$$

typically, a dot product built on some hidden layer of a deep neural network. Similarly to LRP, the model output is propagated backward in the network, layer after layer, until the input features are reached. BiLRP operates by sending messages $R_{jj' \leftarrow kk'}$ from pairs of neurons (k, k') at a given layer to pairs of neurons (j, j') in the layer below.

3.1 Extracting BiLRP Propagation Rules

To build meaningful propagation rules, we make use of the ‘deep Taylor decomposition’ (DTD) [27] framework. DTD expresses the relevance $R_{kk'}$ available for redistribution as a function of activations \mathbf{a} in the layer below. The relation between these two quantities is depicted in Fig. 2. Specifically,

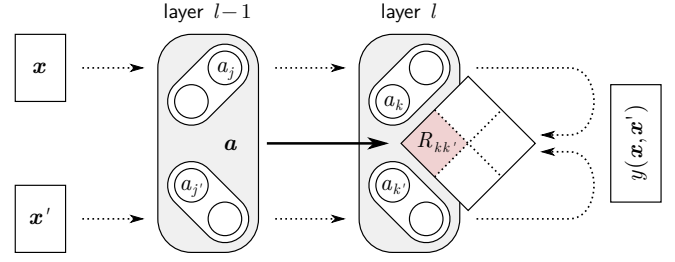


Fig. 2: Diagram of the map used by DTD to derive BiLRP propagation rules. The map connects activations at some layer to relevance in the layer above.

DTD seeks to perform a Taylor expansion of the function $R_{kk'}(\mathbf{a})$ at some reference point $\tilde{\mathbf{a}}$:

$$\begin{aligned} R_{kk'}(\mathbf{a}) &= R_{kk'}(\tilde{\mathbf{a}}) \\ &+ \sum_j [\nabla R_{kk'}(\tilde{\mathbf{a}})]_j \cdot (a_j - \tilde{a}_j) \\ &+ \sum_{j'} [\nabla R_{kk'}(\tilde{\mathbf{a}})]_{j'} \cdot (a_{j'} - \tilde{a}_{j'}) \\ &+ \sum_{jj'} [\nabla^2 R_{kk'}(\tilde{\mathbf{a}})]_{jj'} \cdot (a_j - \tilde{a}_j) (a_{j'} - \tilde{a}_{j'}) \\ &+ \dots \end{aligned}$$

so that messages $R_{jj' \leftarrow kk'}$ can be identified. In practice, the function $R_{kk'}(\mathbf{a})$ is difficult to analyze, because it subsumes a potentially large number of forward and backward computations. DTD introduces the concept of a ‘relevance model’ $\hat{R}_{kk'}(\mathbf{a})$ which locally approximates the true relevance score, but only depends on corresponding activations [27]. For linear/ReLU layers [57], we define the relevance model:

$$\hat{R}_{kk'}(\mathbf{a}) = \underbrace{\left(\sum_j a_j w_{jk} \right)^+}_{a_k} \underbrace{\left(\sum_{j'} a_{j'} w_{j'k'} \right)^+}_{a_{k'}} c_{kk'}$$

with $c_{kk'}$ a constant set in a way that $\hat{R}_{kk'}(\mathbf{a}) = R_{kk'}$. This relevance model is justified later in Proposition 3. We now have an easily analyzable model, more specifically, a model that is bilinear on the joint activated domain and zero elsewhere. We search for a root point $\tilde{\mathbf{a}}$ at the intersection between the two ReLU hinges and the plane $\{\tilde{\mathbf{a}}(t, t') \mid t, t' \in \mathbb{R}\}$ where:

$$\begin{aligned} [\tilde{\mathbf{a}}(t, t')]_j &= a_j - t a_j \cdot (1 + \gamma \cdot \mathbf{1}_{w_{jk} > 0}), \\ [\tilde{\mathbf{a}}(t, t')]_{j'} &= a_{j'} - t' a_{j'} \cdot (1 + \gamma \cdot \mathbf{1}_{w_{j'k'} > 0}) \end{aligned}$$

with $\gamma \geq 0$ a hyperparameter. This search strategy can be understood as starting with the activations \mathbf{a} , and jointly decreasing them (especially the ones with positive contributions) until $\hat{R}_{kk'}(\tilde{\mathbf{a}})$ becomes zero. Zero- and first-order terms of the Taylor expansion vanish, leaving us with the interaction terms $R_{jj' \leftarrow kk'}$. The total relevance received by (j, j') from neurons in the layer above is given by:

$$R_{jj'} = \sum_{kk'} \frac{a_j a_{j'} \rho(w_{jk}) \rho(w_{j'k'})}{\sum_{jj'} a_j a_{j'} \rho(w_{jk}) \rho(w_{j'k'})} R_{kk'} \quad (3)$$

with $\rho(w_{jk}) = w_{jk} + \gamma w_{jk}^+$. A derivation is given in Appendix B.1 of the Supplement. This propagation rule can be seen as a second-order variant of the LRP- γ rule [63] used for explaining DNN classifiers. It has the following

interpretation: A pair of neurons (j, j') is assigned relevance if the following three conditions are met:

- (i) it jointly activates,
- (ii) some pairs of neurons in the layer above jointly react,
- (iii) these reacting pairs are themselves relevant.

In addition to linear/ReLU layers, we would like BiLRP to handle other common layers such as max-pooling and min-pooling. These two layer types can be seen as special cases of the broader class of *positively homogeneous* layers (i.e. satisfying $\forall \mathbf{a} \forall t > 0 : a_k(t\mathbf{a}) = ta_k(\mathbf{a})$). For these layers, the following propagation rule can be derived from DTD:

$$R_{jj'} = \sum_{kk'} \frac{a_j a_{j'} [\nabla^2 a_k a_{k'}]_{jj'}}{\sum_{jj'} a_j a_{j'} [\nabla^2 a_k a_{k'}]_{jj'}} R_{kk'} \quad (4)$$

(cf. Appendix B.2 of the Supplement). This propagation rule has a similar interpretation to the one above, in particular, it also requires for (j, j') to be relevant that the corresponding neurons activate, that some neurons (k, k') in the layer above jointly react, and that the latter neurons are themselves relevant.

3.2 BiLRP as a Composition of LRP Computations

A limitation of a plain application of the propagation rules of Section 3.1 is that we need to handle at each layer a data structure $(R_{kk'})_{kk'}$ which grows quadratically with the number of neurons. Consequently, for large neural networks, a direct computation of these propagation rules is unfeasible. However, it can be shown that relevance scores at each layer can also written in the factored form:

$$\begin{aligned} R_{kk'} &= \sum_{m=1}^h R_{km} R_{k'm} \\ R_{jj'} &= \sum_{m=1}^h R_{jm} R_{j'm} \end{aligned}$$

where h is the dimension of the top-layer feature map, and where the factors can be computed iteratively as:

$$R_{jm} = \sum_k \frac{a_j \rho(w_{jk})}{\sum_j a_j \rho(w_{jk})} R_{km} \quad (5)$$

for linear/ReLU layers, and

$$R_{jm} = \sum_k \frac{a_j [\nabla a_k]_j}{\sum_j a_j [\nabla a_k]_j} R_{km} \quad (6)$$

for positively homogeneous layers. The relevance scores that result from applying these factored computations are strictly equivalent to those one would get if using the original propagation rules of Section 3.1. A proof is given in Appendix C of the Supplement.

Furthermore, in comparison to the $(\# \text{ neurons})^2$ computations required at each layer by the original propagation rules, the factored formulation only requires $(\# \text{ neurons} \times 2h)$ computations. The factored form is therefore especially advantageous when h is low. In the experiments of Section 5, we will improve the explanation runtime of our similarity models by adding an extra layer projecting output activations to a smaller number of dimensions.

Lastly, we observe that Equations (5) and (6) correspond to common rules used by standard LRP. The first one is equivalent to the LRP- γ rule [63] used in convolution/ReLU

layers of DNN classifiers. The second one corresponds to the way LRP commonly handles pooling layers [24]. These propagation rules apply independently on each branch and factor of the similarity model. This implies that BiLRP can be implemented as a combination of multiple LRP procedures that are then recombined once the input layer has been reached:

$$\text{BiLRP}(y, \mathbf{x}, \mathbf{x}') = \sum_{m=1}^h \text{LRP}([\phi_L \circ \dots \circ \phi_1]_m, \mathbf{x}) \otimes \text{LRP}([\phi_L \circ \dots \circ \phi_1]_m, \mathbf{x}')$$

This modular approach to compute BiLRP explanations is shown graphically in Fig. 3.

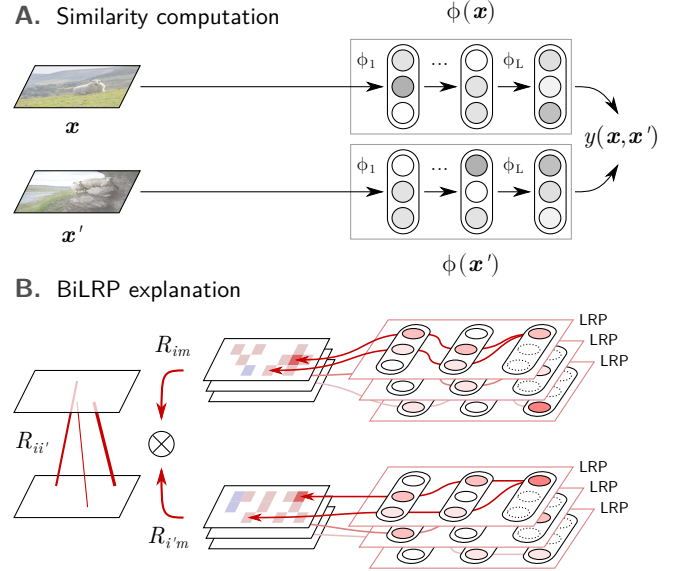


Fig. 3: Illustration of our approach to compute BiLRP explanations: **A.** Input examples are mapped by the neural network up to the layer at which the similarity model is built. **B.** LRP is applied to all individual activations in this layer, and the resulting array of explanations is recombined into a single explanation of predicted similarity.

With this modular structure, BiLRP can be easily and efficiently implemented based on existing explanation software. We note that the modular approach described here is not restricted to LRP. Other explanation techniques could in principle be used in the composition. Doing so would however lose the interpretation of the explanation procedure as a deep Taylor decomposition.

3.3 Theoretical Properties of BiLRP

A number of results can be shown about BiLRP. A first result relates the produced explanation to the predicted similarity. Another result lets us view the Hessian \times Product method as a special case of BiLRP. A last result provides a justification for the relevance models used in Section 3.1.

Proposition 1. For deep rectifier networks with zero biases, BiLRP is conservative, i.e. $\sum_{ii'} R_{ii'} = y(\mathbf{x}, \mathbf{x}')$.

(See Appendix D.1 of the Supplement for a proof.) Conservation ensures that relevance scores are in proportion to the output of the similarity model.

Proposition 2. When $\gamma = 0$, explanations produced by BiLRP reduce to those of Hessian \times Product.

(See Appendix D.2 of the Supplement for a proof.) We will find in Section 4 that choosing non-zero values of γ gives better explanations.

Proposition 3. The relevance computed by BiLRP at each layer can be rewritten as $R_{jj'} = a_j a_{j'} c_{jj'}$, where $c_{jj'}$ is locally approximately constant.

(Cf. Appendix D.3 of the Supplement.) This property supports the modeling of $c_{jj'}, c_{kk'}, \dots$ as constant, leading to easily analyzable relevance models from which the BiLRP propagation rules of Section 3.1 can be derived.

4 BiLRP VS. BASELINES

This section tests the ability of the proposed BiLRP method to produce faithful explanations. In general, ground-truth explanations of ML predictions, especially nonlinear ones, are hard to acquire [22], [64]. Thus, we consider an *artificial* scenario consisting of:

- (i) a hardcoded similarity model from which it is easy to extract ground-truth explanations,
- (ii) a neural network trained to reproduce the hardcoded model exactly on the whole input domain.

Because the hardcoded model and the neural network become exact functional copies after training, explanations for their predictions should be the same. Hence, this gives us ground-truth explanations to evaluate BiLRP against baseline methods.

The hardcoded similarity model takes two random sequences of 6 digits as input and counts the number of matches between them. The matches between the two sequences form the ground truth explanation. The neural network is constructed and trained as follows: Each digit forming the sequence is represented as vectors in \mathbb{R}_+^{10} . To avoid a too simple task, we set these vectors to be correlated. Vectors associated to the digits in the sequence are then concatenated to form an input $\mathbf{x} \in \mathbb{R}_+^{6 \times 10}$. The input goes through two hidden layers of size 100 and one top layer of size 50 corresponding to the feature map. We train the network for 10000 iterations of stochastic gradient descent to minimize the mean square error between predictions and ground-truth similarities, and reach an error of 10^{-3} , indicating that the neural network solves the problem perfectly.

Because there is currently no well-established method for explaining similarity, we consider three simple baselines and use them as a benchmark for evaluating BiLRP:

- ‘Saliency’: $R_{ii'} = (x_i x_{i'})^2$
- ‘Curvature’: $R_{ii'} = ([\nabla^2 y(\mathbf{x}, \mathbf{x}')]_{ii'})^2$
- ‘Hessian \times Product’: $R_{ii'} = x_i x_{i'} [\nabla^2 y(\mathbf{x}, \mathbf{x}')]_{ii'}$

Each explanation method produces a scoring over all pairs of input features, i.e. a $(6 \times 10) \times (6 \times 10)$ -dimensional explanation. The latter can be pooled over embedding dimensions (cf. Appendix E of the Supplement) to form a 6×6 matrix connecting the digits from the two sequences. Results are shown in Fig. 4. The closer the produced connectivity pattern to the ground truth, the better the explanation method.

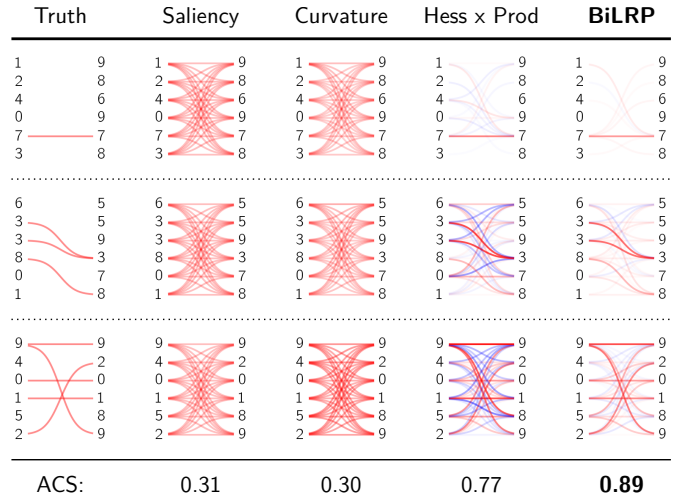


Fig. 4: Benchmark comparison on a toy example where we have ground-truth explanation of similarity. BiLRP performs better than all baselines, as measured by the average cosine similarity to the ground truth.

High scores are shown in red, low scores in light red or white, and negative scores in blue.

We observe that the ‘Saliency’ baseline does not differentiate between matching and non-matching digits. This is explained by the fact that this baseline is not output-dependent and thus does not know the task. The ‘Curvature’ baseline, although sensitive to the output, does not improve over saliency. The ‘Hessian \times Product’ baseline, which can be seen as a special case of BiLRP with $\gamma = 0$, matches the ground truth more accurately but introduces some spurious negative contributions. BiLRP, through a proper choice of parameter γ (here set to 0.09) considerably reduces these negative contributions.

This visual inspection is validated quantitatively by considering a large number of examples and computing the average cosine similarity (ACS) between the produced explanations and the ground truth. An ACS of 1.0 indicates perfect matching with the ground truth. ‘Saliency’ and ‘Curvature’ baselines have low ACS. The accuracy is strongly improved by ‘Hessian \times Product’ and further improved by BiLRP. The effect of the parameter γ of BiLRP on the ACS score is shown in Fig. 5.

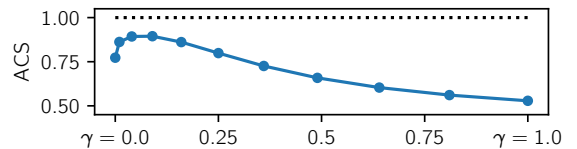


Fig. 5: Effect of the BiLRP parameter γ on the average cosine similarity between the explanations and the ground truth.

We observe that the best parameter γ is small but non-zero. Like for standard LRP, the explanation can be further fine-tuned, e.g. by setting the parameter γ different at each layer or by considering a broader set of LRP propagation rules [65], [63].

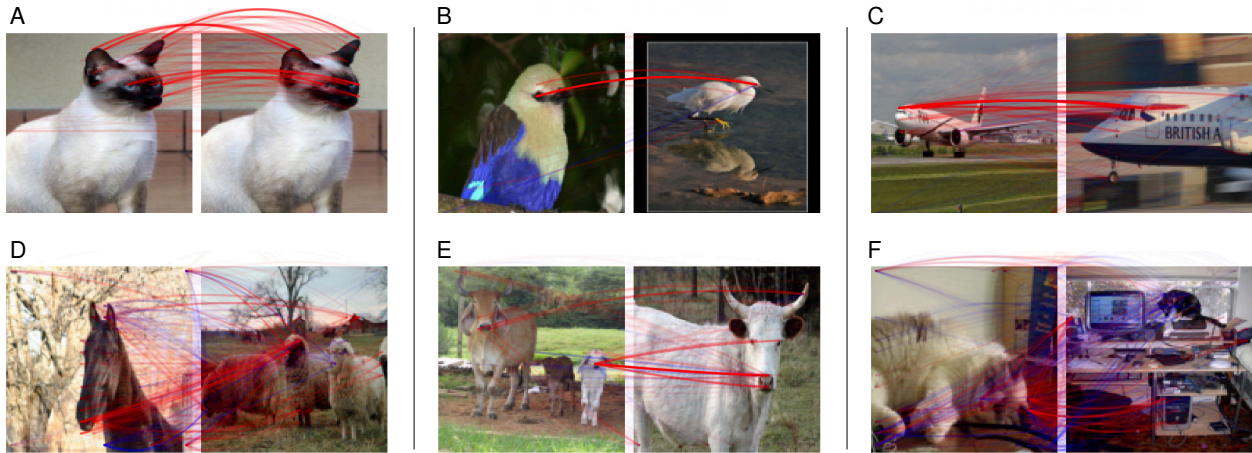


Fig. 6: Application of BiLRP to a dot-product similarity model built on VGG-16 features at layer 31. BiLRP identifies patterns in the data (e.g. ears, eyes) that contribute to the modeled similarity.

5 INTERPRETING DEEP SIMILARITY MODELS

Our next step will be to use BiLRP to gain insight into practical similarity models built on the well-established VGG-16 convolutional neural network [28]. We take a pretrained version of this network and build the similarity model

$$y(\mathbf{x}, \mathbf{x}') = \langle \text{VGG}_{:31}(\mathbf{x}), \text{VGG}_{:31}(\mathbf{x}') \rangle,$$

i.e. a dot product on the neural network activations at layer 31. This layer corresponds to the last layer of features before the classifier. The mapping from input to layer 31 is a sequence of convolution/ReLU layers, and max-pooling layers. It is therefore explainable by BiLRP. However, the large number of dimensions entering in the dot product computation (512 feature maps of size $\frac{w}{32} \times \frac{h}{32}$) where w and h are the dimensions of the input image, makes a direct application of BiLRP computationally expensive. To reduce the computation time, we append to the last layer a random projection layer that maps activations to a lower-dimensional subspace. In our experiments, we find that projecting to 100 dimensions provides sufficiently detailed explanations and achieves the desired computational speedup. We set the BiLRP parameter γ to 0.5, 0.25, 0.1, 0.0 for layers 2–10, 11–17, 18–24, 25–31 respectively. For layer 1, we use the z^B -rule, that specifically handles the pixel-domain [27]. Finally, we apply a 8×8 pooling on the output of BiLRP to reduce the size of the explanations. Details of the rendering procedure are given in Appendix F of the Supplement.

Figure 6 shows our BiLRP explanations on a selection of images pairs taken from the Pascal VOC 2007 dataset [66] and resized to 128×128 pixels. Positive relevance scores are shown in red, negative scores in blue, and score magnitude is represented by opacity. Example A shows two identical images being compared. BiLRP finds that eyes, nose, and ears are the most relevant features to explain similarity. Example B shows two different images of birds. Here, the eyes are again contributing to the high similarity. In Example C, the front part of the two planes are matched.

Examples D and E show cases where the similarity is not attributed to what the user may expect. In Example D,

the horse’s muzzle is matched to the head of a sheep. In Example E, while we expect the matching to occur between the two large animals in the image, the true reason for similarity is a small white calf in the right part of the first image. In example F, the scene is cluttered, and does not let appear any meaningful similarity structure, in particular, the two cats are not matched. We also see in this last example that a substantial amount of negative relevance appears, indicating that several joint patterns contradict the similarity score.

Overall, the BiLRP method gives insight into the strengths and weaknesses of a similarity model, by revealing the features and their relative poses/locations that the model is able or not able to match.

5.1 How Transferable is the Similarity Model?

Deep neural networks, through their multiple layers of representation, provide a natural framework for multi-task/transfer learning [67], [68]. DNN-based transfer learning has seen many successful applications [69], [70], [71]. In this section, we consider the problem of transferring a *similarity* model to some task of interest. We will use BiLRP to compare different similarity models, and show how their transferability can be assessed visually from the explanations.

We take the pretrained VGG-16 model and build dot product similarity models at layers 5, 10, 17, 24, 31 (i.e. after each max-pooling layer):

$$\begin{aligned} y^{(5)}(\mathbf{x}, \mathbf{x}') &= \langle \text{VGG}_{:5}(\mathbf{x}), \text{VGG}_{:5}(\mathbf{x}') \rangle, \\ &\vdots \\ y^{(31)}(\mathbf{x}, \mathbf{x}') &= \langle \text{VGG}_{:31}(\mathbf{x}), \text{VGG}_{:31}(\mathbf{x}') \rangle \end{aligned}$$

Like in the previous experiment, we add to each feature representation a random projection onto 100 dimensions in order to make explanations faster to compute. In the following experiments, we consider transfer of similarity to the following three datasets:

- ‘Unconstrained Facial Images’ (UFI) [72],
- ‘Labeled Faces in the Wild’ (LFW) [73],
- ‘The Sphaera Corpus’ [29], [74].

The first two datasets are face identification tasks. In identification tasks, a good similarity model is needed in order to reliably extract the closest matches in the training data [50], [75]. The third dataset is composed of 358 scanned academic textbooks from the 15th to the 17th century containing texts, illustrations and tables related to astronomical studies. Again, similarity between these entities is important, as it can serve to consolidate historical networks [53], [76], [77].

Faces and illustrations are fed to the neural network as images of size 64×64 pixels and 96×96 pixels respectively. We choose for each dataset a pair composed of a test example and the most similar training example. For each pair, we compute the BiLRP explanations. Results for the similarity model at layer 17 and 31 are shown in Fig. 7.

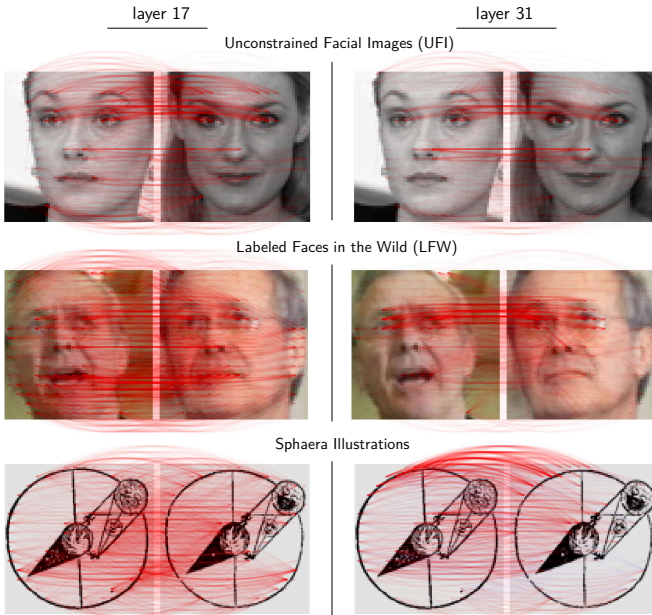


Fig. 7: Application of BiLRP to study how VGG-16 similarity transfers to various datasets.

We observe that the explanation of similarity at layer 31 is focused on a limited set of features: the eyes or the nose on face images, and a reduced set of lines on the Sphaera illustrations. In comparison, explanations of similarity at layer 17 cover a broader set of features. These observations suggest that similarity in highest layers, although being potentially capable of resolving very fine variations (e.g. for the eyes), might not have kept sufficiently many features in other regions, in order to match images accurately.

To verify this hypothesis, we train a collection of linear SVMs on each dataset where each SVM takes as input activations at a particular layer. On the UFI dataset, we use the original training and test sets. On LFW and Sphaera, data points are assigned randomly with equal probability to the training and test set. The hyperparameter C of the SVM is selected by grid search from the set of values $\{0.001, 0.01, 0.1, 1, 10, 100, 1000\}$ over 4 folds on the training set. Test set accuracies for each dataset and layer are shown in Table 1.

These results corroborate the hypothesis initially constructed from the BiLRP explanations: Overspecialization

TABLE 1: Accuracy of a SVM built on different layers of the VGG-16 network and for different datasets.

dataset	# classes	layer				
		5	10	17	24	31
UFI	605	0.45	0.57	0.62	0.54	0.19
LFW	61	0.78	0.86	0.92	0.89	0.75
Sphaera	111	0.93	0.96	0.98	0.97	0.96

of top layers on the original task leads to a sharp drop of accuracy on the target task. Best accuracies are instead obtained in the intermediate layers.

5.2 How *Invariant* is the Similarity Model?

To further demonstrate the potential of BiLRP for characterizing a similarity model, we consider the problem of assessing its invariance properties. Representations that incorporate meaningful invariance are particularly desirable as they enable learning and generalizing from fewer data points [78], [79].

Invariance can however be difficult to measure in practice: On one hand, the model should respond equally to the input and its transformed version. On the other hand, the response should be selective [80], [81], i.e. not the same for every input. In the context of neural networks, a proposed measure of invariance that implements this joint requirement is the local/global firing ratio [81]. In a similar way, we consider an invariance measure for similarity models based on the local/global similarity ratio:

$$\text{INV} = \frac{\langle y(\mathbf{x}, \mathbf{x}') \rangle_{\text{local}}}{\langle y(\mathbf{x}, \mathbf{x}') \rangle_{\text{global}}} \quad (7)$$

The expression $\langle \cdot \rangle_{\text{local}}$ denotes an average over pairs of transformed points (which our model should predict to be similar), and $\langle \cdot \rangle_{\text{global}}$ denotes an average over all pairs of points.

We study the layer-wise forming of invariance in the VGG-16 network. We use for this the ‘UCF Sports Action’ video dataset [82], [83], where consecutive video frames readily provide a wealth of transformations (translation, rotation, rescaling, etc.) which we would like our model to be invariant to, i.e. produce a high similarity score. Videos are cropped to square shape and resized to size 128×128 . We define $\langle \cdot \rangle_{\text{local}}$ to be the average over pairs of nearby frames in the same video ($\Delta t \leq 5$), and $\langle \cdot \rangle_{\text{global}}$ to be the average over all pairs, also from different videos. Invariance scores obtained for similarity models built at various layers are shown in Table 2.

TABLE 2: Invariance measured by Eq. (7) at various layers of the VGG-16 network on the UCF Sports Action dataset.

	layer				
	5	10	17	24	31
INV	2.30	2.31	2.43	2.87	4.00

Invariance increases steadily from the lower to the top layers of the neural network and reaches a maximum score

at layer 31. We now take a closer look at the invariance score in this last layer, by applying the following two steps:

- (i) The invariance score is decomposed on the pairs of video frames that directly contribute to it, i.e. through the term $\langle \cdot \rangle_{\text{local}}$ of Eq. (7).
- (ii) BiLRP is applied to these pairs of contributing video frames in order to produce a finer pixel-wise explanation of invariance.

This two-step analysis is shown in Fig. 8 for a selection of videos and pairs of video frames.

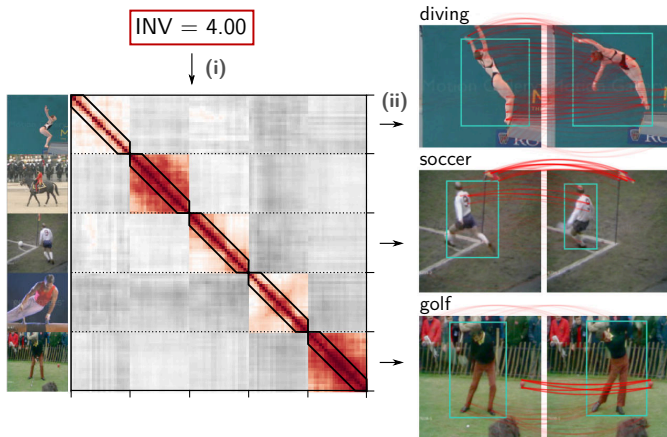


Fig. 8: Explanation of measured invariance at layer 31. *Left*: Similarity matrix associated to a selection of video clips. The diagonal band outlined in black contains the pairs of examples in $\langle \cdot \rangle_{\text{local}}$. *Right*: BiLRP explanations for selected pairs from the diagonal band.

The first example shows a diver rotating counterclockwise as she leaves the platform. Here, the contribution to invariance is meaningfully attributed to the different parts of the rotating body. The second example shows a soccer player performing a corner kick. Part of the invariance is attributed to the player moving from right to left, however, a sizable amount of it is also attributed in an unexpected manner to the static corner flag behind the soccer player. The last example shows a golf player as he strikes the ball. Again, invariance is unexpectedly attributed to a small red object in the grass. This small object would have likely been overlooked, even after a preliminary inspection of the input images.

The reliance of the invariance measure on unexpected objects in the image (corner flag, small red object) can be viewed as a ‘Clever Hans’ effect [19]: the observer assesses how ‘intelligent’ (or invariant) the model is, based on looking at the outcome of a given experiment (the computed invariance score), instead of investigating the decision structure that leads to the high invariance score. This effect may lead to an overestimation of the invariance properties of the model.

Similar ‘Clever Hans’ effects can also be observed beyond video data, e.g. when applying the similarity model to illustrations in the Sphaera corpus. Figure 9 shows two pairs of illustrations whose content is equivalent up to a rotation, and for which our model predicts a high similarity.

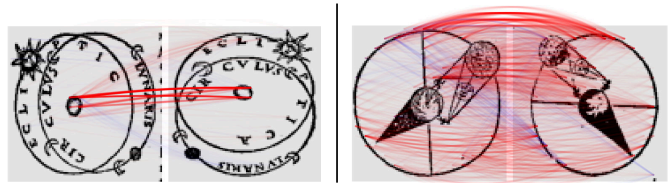


Fig. 9: Pairs of illustrations from the Sphaera corpus, explained with BiLRP. The high similarity originates mainly from matching fixed features in the image rather than capturing the rotating elements.

Once more, BiLRP reveals in both cases that the high similarity is not due to matching the rotated patterns, but mainly fixed elements at the center and at the border of the image respectively.

Overall, we have demonstrated that BiLRP can be useful to identify unsuspected and potentially undesirable reasons for high measured invariance. Practically, applying this method can help to avoid deploying a model with false expectations in real-world applications. Our analysis also suggests that better *explanation-based* invariance measures could be designed in the future, potentially in combination with optical flows [84], in order to better distinguish between the matching structures that should and should not contribute to the invariance score.

6 ENGINEERING EXPLAINABLE SIMILARITIES

In this section, we turn to an open and significant problem in the digital humanities: assessing similarity between numeric tables in historical textbooks. We consider scanned numeric tables from the Sphaera Corpus [29]. Tables contained in the corpus typically report astronomical measurements or calculations of the positions of celestial objects in the sky. Examples of such tables are given in Fig. 10 A. Producing an accurate model of similarity between astronomical tables would allow to further consolidate historical networks, which would in turn allow for better inferences.

The similarity prediction task has so far proved challenging: First, it is difficult to acquire ground truth similarity. Getting similarity labels would require a meticulous inspection by a human expert of potentially large tables, and the process would need to be repeated for many of pairs of tables. Also, unlike natural images, faces, or illustrations, which are all well represented by existing pretrained convolutional neural networks, table data usually requires ad-hoc approaches [85], [86]. In particular, we need to specify which aspects of the tables (e.g. numbers, style, or layout) should support the similarity.

6.1 The ‘Bigram Network’

We propose a novel ‘bigram network’ to predict table similarity. Our network can be learned from very few human annotations and is designed to encourage the prediction to be based on relevant numerical features. The network consists of two parts:

The first part is a standard stack of convolution/ReLU layers taking a scanned table x as input and producing 10

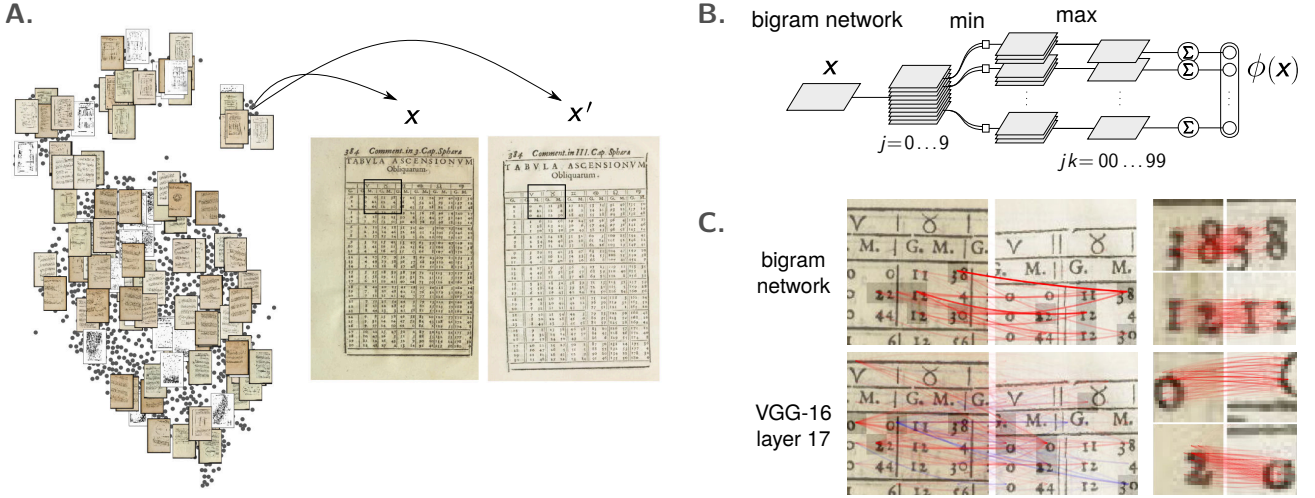


Fig. 10: **A.** Collection of tables from the Sphaera Corpus [29] from which we extract two tables with identical content. **B.** Proposed ‘bigram network’ supporting the table similarity model. **C.** BiLRP explanations of predicted similarities between the two input tables.

activation maps $\{a_j(\mathbf{x})\}_{j=1}^{10}$ detecting the digits 0–9. The map $a_j(\mathbf{x})$ is trained to produce small Gaussian blobs at locations where digits of class j are present. The convolutional network is trained on a few hundreds of single digit labels along with their respective image patches. We also incorporate a comparable amount of negative examples (from non-table pages) to correctly handle the absence of digits.

The second part of the network is a hard-coded sequence of layers that extracts task-relevant information from the single-digit activation maps. The first layer in the sequence performs an element-wise ‘min’ operation:

$$\mathbf{a}_{jk}^{(\tau)}(\mathbf{x}) = \min \{a_j(\mathbf{x}), \tau(a_k(\mathbf{x}))\}$$

The ‘min’ operation can be interpreted as a continuous ‘AND’ [38], and tests at each location for the presence of bigrams $jk \in 00\text{--}99$. The function τ represents some translation operation, and we apply several of them to produce candidate alignments between the digits forming the bigrams (e.g. horizontal shifts of 8, 10, and 12 pixels). We then apply the max-pooling layer:

$$\mathbf{a}_{jk}(\mathbf{x}) = \max_{\tau} \{a_{jk}^{(\tau)}(\mathbf{x})\}.$$

The ‘max’ operation can be interpreted as a continuous ‘OR’, and determines at each location whether a bigram has been found for at least one candidate alignment. Finally, a global sum-pooling layer is applied spatially:

$$\phi_{jk}(\mathbf{x}) = \|\mathbf{a}_{jk}(\mathbf{x})\|_1$$

It introduces global translation invariance into the model and produces a 100-dimensional output vector representing the sum of activations for each bigram. The bigram network is depicted in Fig. 10 B.

From the output of the bigram network, the similarity score can be obtained by applying the dot product $y(\mathbf{x}, \mathbf{x}') = \langle \phi(\mathbf{x}), \phi(\mathbf{x}') \rangle$. Furthermore, because the bigram

network is exclusively composed of convolution/ReLU layers and standard pooling operations, similarities built at the output of this network remain fully explainable by BiLRP.

6.2 Validating the ‘Bigram Network’ with BiLRP

We come to the final step which is to validate the ‘bigram network’ approach on the task of predicting table similarity. Examples of common validation procedures include precision-recall curves, or the ability to solve a proxy task (e.g. table classification) from the predicted similarities. These validation procedures require label information, which is however difficult to obtain for this type of data. Furthermore, when the labeled data is not sufficiently representative, these procedures are potentially affected by the ‘Clever Hans’ effect [19].

In the following, we will show that BiLRP, through the explanatory feedback it provides, offers a much more data efficient way of performing model validation. We take a pair of tables (\mathbf{x}, \mathbf{x}'), which a preliminary manual inspection has verified to be similar. We then apply BiLRP to explain:

- (i) the similarity score at the output of our engineered task-specific ‘bigram network’,
- (ii) the similarity score at layer 17 of a generic pretrained VGG-16 network.

For the bigram network, the BiLRP parameter γ is set to 0.5 at each convolution layer. For the VGG-16 network, we use the same BiLRP parameters as in Section 5. The result of our analysis is shown in Fig. 10 C.

The bigram network similarity model correctly matches pairs of digits in the two tables. Furthermore, matches are produced between sequences occurring at different locations, thereby verifying the structural translation invariance of the model. Pixel-level explanations further validate the approach by showing that individual digits are matched in a meaningful manner. In contrast, the similarity model built on VGG-16 does not distinguish between the different pairs of digits. Furthermore, part of the similarity score is

supported by aspects that are not task-relevant, such as table borders.—Hence, for this particular table similarity task, BiLRP can clearly establish the superiority of the bigram network over VGG-16.

We stress that this assessment could be readily obtained from a *single* pair of tables. If instead we would have applied a validation technique that relies only on similarity scores, significantly more data would have been needed in order to reach the same conclusion with confidence. This sample efficiency of BiLRP (and by extension any successful explanation technique) for the purpose of model validation is especially important in digital humanities or other scientific domains, where ground-truth labels are typically scarce or expensive to obtain.

7 CONCLUSION

Similarity is a central concept in machine learning that is precursor to a number of supervised and unsupervised machine learning methods. In this paper, we have shown that it can be crucial to get a human-interpretable explanation of the predicted similarity before using it to train a practical machine learning model.

We have contributed a theoretically well-founded method to explain similarity in terms of pairs of input features. Our method called BiLRP can be expressed as a composition of LRP computations. It therefore inherits its robustness and broad applicability, but extends it to the novel scenario of similarity explanation.

The usefulness of BiLRP was showcased on the task of understanding similarities as implemented by the VGG-16 neural network, where it could predict transfer learning capabilities and highlight clear cases of ‘Clever Hans’ [19] predictions. Furthermore, for a practically relevant problem in the digital humanities, BiLRP was able to demonstrate with very limited data the superiority of a task-specific similarity model over a generic VGG-16 solution.

Future work will extend the presented techniques from binary towards n-ary similarity structures, especially aiming at incorporating the different levels of reliability of the input features. Furthermore we will use the proposed research tool to gain insight into large data collections, in particular, grounding historical networks to interpretable domain-specific concepts.

ACKNOWLEDGEMENTS

This work was funded by the German Ministry for Education and Research as BIFOLD – Berlin Institute for the Foundations of Learning and Data (ref. 01IS18025A and ref. 01IS18037A), and the German Research Foundation (DFG) as Math+: Berlin Mathematics Research Center (EXC 2046/1, project-ID: 390685689). This work was partly supported by the Institute for Information & Communications Technology Planning & Evaluation (IITP) grant funded by the Korea government (No. 2017-0-00451, No. 2017-0-01779).

REFERENCES

- [1] A. Zien, G. Rätsch, S. Mika, B. Schölkopf, T. Lengauer, and K.-R. Müller, “Engineering support vector machine kernels that recognize translation initiation sites,” *Bioinformatics*, vol. 16, no. 9, pp. 799–807, 2000.

- [2] C. D. Manning, P. Raghavan, and H. Schütze, *Introduction to information retrieval*. Cambridge University Press, 2008.
- [3] A. Nierman and H. V. Jagadish, “Evaluating structural similarity in XML documents,” in *WebDB*, 2002, pp. 61–66.
- [4] E. Pampalk, A. Flexer, and G. Widmer, “Improvements of audio-based music similarity and genre classification,” in *ISMIR*, 2005, pp. 628–633.
- [5] P. Willett, J. M. Barnard, and G. M. Downs, “Chemical similarity searching,” *Journal of Chemical Information and Computer Sciences*, vol. 38, no. 6, pp. 983–996, 1998.
- [6] C. M. Bishop, *Pattern Recognition and Machine Learning (Information Science and Statistics)*. Berlin, Heidelberg: Springer-Verlag, 2006.
- [7] B. Schölkopf and A. J. Smola, *Learning with kernels: support vector machines, regularization, optimization, and beyond*, ser. Adaptive computation and machine learning series. MIT Press, 2002.
- [8] J. MacQueen, “Some methods for classification and analysis of multivariate observations,” in *Proceedings of the Fifth Berkeley Symposium on Mathematical Statistics and Probability, Volume 1: Statistics*. Berkeley, Calif.: University of California Press, 1967, pp. 281–297.
- [9] A. K. Jain, M. N. Murty, and P. J. Flynn, “Data clustering: A review,” *ACM Comput. Surv.*, vol. 31, no. 3, pp. 264–323, 1999.
- [10] J. Shi and J. Malik, “Normalized cuts and image segmentation,” *IEEE Trans. Pattern Anal. Mach. Intell.*, vol. 22, no. 8, pp. 888–905, 2000.
- [11] B. Schölkopf, J. C. Platt, J. Shawe-Taylor, A. J. Smola, and R. C. Williamson, “Estimating the support of a high-dimensional distribution,” *Neural Computation*, vol. 13, no. 7, pp. 1443–1471, 2001.
- [12] B. Schölkopf, A. J. Smola, and K.-R. Müller, “Nonlinear component analysis as a kernel eigenvalue problem,” *Neural Computation*, vol. 10, no. 5, pp. 1299–1319, 1998.
- [13] T. Mikolov, I. Sutskever, K. Chen, G. S. Corrado, and J. Dean, “Distributed representations of words and phrases and their compositionality,” in *NIPS*, 2013, pp. 3111–3119.
- [14] L. van der Maaten and G. E. Hinton, “Visualizing non-metric similarities in multiple maps,” *Machine Learning*, vol. 87, no. 1, pp. 33–55, 2012.
- [15] F. R. Bach, G. R. G. Lanckriet, and M. I. Jordan, “Multiple kernel learning, conic duality, and the SMO algorithm,” in *ICML*, ser. ACM International Conference Proceeding Series, vol. 69. ACM, 2004.
- [16] S. Sonnenburg, G. Rätsch, C. Schäfer, and B. Schölkopf, “Large scale multiple kernel learning,” *J. Mach. Learn. Res.*, vol. 7, pp. 1531–1565, 2006.
- [17] K. Q. Weinberger and L. K. Saul, “Distance metric learning for large margin nearest neighbor classification,” *J. Mach. Learn. Res.*, vol. 10, pp. 207–244, 2009.
- [18] J. Bergstra and Y. Bengio, “Random search for hyper-parameter optimization,” *J. Mach. Learn. Res.*, vol. 13, pp. 281–305, 2012.
- [19] S. Lapuschkin, S. Wäldchen, A. Binder, G. Montavon, W. Samek, and K.-R. Müller, “Unmasking Clever Hans predictors and assessing what machines really learn,” *Nature Communications*, vol. 10, p. 1096, 2019.
- [20] W. Samek, G. Montavon, A. Vedaldi, L. K. Hansen, and K.-R. Müller, Eds., *Explainable AI: Interpreting, Explaining and Visualizing Deep Learning*, ser. Lecture Notes in Computer Science. Springer, 2019, vol. 11700.
- [21] Z. C. Lipton, “The mythos of model interpretability,” *Commun. ACM*, vol. 61, no. 10, pp. 36–43, 2018.
- [22] G. Montavon, W. Samek, and K.-R. Müller, “Methods for interpreting and understanding deep neural networks,” *Digital Signal Processing*, vol. 73, pp. 1–15, 2018.
- [23] D. Baehrens, T. Schroeter, S. Harmeling, M. Kawanabe, K. Hansen, and K.-R. Müller, “How to explain individual classification decisions,” *J. Mach. Learn. Res.*, vol. 11, pp. 1803–1831, 2010.
- [24] S. Bach, A. Binder, G. Montavon, F. Klauschen, K.-R. Müller, and W. Samek, “On pixel-wise explanations for non-linear classifier decisions by layer-wise relevance propagation,” *PLoS ONE*, vol. 10, no. 7, p. e0130140, 07 2015.
- [25] M. T. Ribeiro, S. Singh, and C. Guestrin, “‘Why should I trust you?’: Explaining the predictions of any classifier,” in *KDD*. ACM, 2016, pp. 1135–1144.
- [26] R. R. Selvaraju, M. Cogswell, A. Das, R. Vedantam, D. Parikh, and D. Batra, “Grad-CAM: Visual explanations from deep networks via gradient-based localization,” in *ICCV*. IEEE Computer Society, 2017, pp. 618–626.
- [27] G. Montavon, S. Lapuschkin, A. Binder, W. Samek, and K.-R. Müller, “Explaining nonlinear classification decisions with deep

- Taylor decomposition," *Pattern Recognition*, vol. 65, pp. 211–222, 2017.
- [28] K. Simonyan and A. Zisserman, "Very deep convolutional networks for large-scale image recognition," in *ICLR*, 2015.
- [29] M. Valleriani, F. Kräutli, M. Zamani, A. Tejedor, C. Sander, M. Vogl, S. Bertram, G. Funke, and H. Kantz, "The emergence of epistemic communities in the sphaera corpus: Mechanisms of knowledge evolution," *Journal of Historical Network Research*, vol. 3, pp. 50–91, 2019.
- [30] S. T. Roweis and L. K. Saul, "Nonlinear Dimensionality Reduction by Locally Linear Embedding," *Science*, vol. 290, no. 5500, pp. 2323–2326, 2000.
- [31] R. R. Coifman and S. Lafon, "Diffusion maps," *Applied and Computational Harmonic Analysis*, vol. 21, no. 1, pp. 5–30, Jul. 2006.
- [32] M. D. Zeiler and R. Fergus, "Visualizing and understanding convolutional networks," in *ECCV (1)*, ser. Lecture Notes in Computer Science, vol. 8689. Springer, 2014, pp. 818–833.
- [33] L. M. Zintgraf, T. S. Cohen, T. Adel, and M. Welling, "Visualizing deep neural network decisions: Prediction difference analysis," in *ICLR (Poster)*. OpenReview.net, 2017.
- [34] S. M. Lundberg and S. Lee, "A unified approach to interpreting model predictions," in *NIPS*, 2017, pp. 4765–4774.
- [35] K. Simonyan, A. Vedaldi, and A. Zisserman, "Deep inside convolutional networks: Visualising image classification models and saliency maps," in *ICLR (Workshop Poster)*, 2014.
- [36] D. Smilkov, N. Thorat, B. Kim, F. B. Viégas, and M. Wattenberg, "SmoothGrad: removing noise by adding noise," *CoRR*, vol. abs/1706.03825, 2017.
- [37] M. Sundararajan, A. Taly, and Q. Yan, "Axiomatic attribution for deep networks," in *ICML*, ser. Proceedings of Machine Learning Research, vol. 70. PMLR, 2017, pp. 3319–3328.
- [38] J. Kauffmann, K.-R. Müller, and G. Montavon, "Towards explaining anomalies: A deep Taylor decomposition of one-class models," *Pattern Recognition*, p. 107198, 2020.
- [39] B. Micenková, R. T. Ng, X. Dang, and I. Assent, "Explaining outliers by subspace separability," in *ICDM*. IEEE Computer Society, 2013, pp. 518–527.
- [40] J. Kauffmann, M. Esders, G. Montavon, W. Samek, and K.-R. Müller, "From clustering to cluster explanations via neural networks," *CoRR*, vol. abs/1906.07633, 2019.
- [41] M. Tsang, D. Cheng, and Y. Liu, "Detecting statistical interactions from neural network weights," in *ICLR (Poster)*. OpenReview.net, 2018.
- [42] T. Cui, P. Marttinen, and S. Kaski, "Recovering pairwise interactions using neural networks," *CoRR*, vol. abs/1901.08361, 2019.
- [43] S. Leupold, "Second-order Taylor decomposition for explaining spatial transformation of images," Master's thesis, Technische Universität Berlin, 2017.
- [44] R. Caruana, Y. Lou, J. Gehrke, P. Koch, M. Sturm, and N. Elhadad, "Intelligible models for healthcare: Predicting pneumonia risk and hospital 30-day readmission," in *KDD*. ACM, 2015, pp. 1721–1730.
- [45] J. D. Janizek, P. Sturmfels, and S. Lee, "Explaining explanations: Axiomatic feature interactions for deep networks," *CoRR*, vol. abs/2002.04138, 2020.
- [46] C. Watkins, "Dynamic alignment kernels," in *Advances in Large Margin Classifiers*. MIT Press, 1999, pp. 39–50.
- [47] K. Tsuda, M. Kawanabe, G. Rätsch, S. Sonnenburg, and K.-R. Müller, "A new discriminative kernel from probabilistic models," *Neural Computation*, vol. 14, no. 10, pp. 2397–2414, 2002.
- [48] T. Gärtner, "A survey of kernels for structured data," *SIGKDD Explorations*, vol. 5, no. 1, pp. 49–58, 2003.
- [49] J. Bromley, I. Guyon, Y. LeCun, E. Säckinger, and R. Shah, "Signature verification using a siamese time delay neural network," in *NIPS*. Morgan Kaufmann, 1993, pp. 737–744.
- [50] S. Chopra, R. Hadsell, and Y. LeCun, "Learning a similarity metric discriminatively, with application to face verification," in *CVPR (1)*. IEEE Computer Society, 2005, pp. 539–546.
- [51] J. Wang, Y. Song, T. Leung, C. Rosenberg, J. Wang, J. Philbin, B. Chen, and Y. Wu, "Learning fine-grained image similarity with deep ranking," in *CVPR*. IEEE Computer Society, 2014, pp. 1386–1393.
- [52] E. Hoffer and N. Ailon, "Deep metric learning using triplet network," in *SIMBAD*, ser. Lecture Notes in Computer Science, vol. 9370. Springer, 2015, pp. 84–92.
- [53] B. Seguin, C. Striolo, I. diLenardo, and F. Kaplan, "Visual link retrieval in a database of paintings," in *ECCV Workshops (1)*, ser. Lecture Notes in Computer Science, vol. 9913. Springer, 2016, pp. 753–767.
- [54] X. He, L. Liao, H. Zhang, L. Nie, X. Hu, and T. Chua, "Neural collaborative filtering," in *WWW*. ACM, 2017, pp. 173–182.
- [55] R. Memisevic and G. E. Hinton, "Learning to represent spatial transformations with factored higher-order Boltzmann machines," *Neural Computation*, vol. 22, no. 6, pp. 1473–1492, 2010.
- [56] K. Tzompanaki and M. Doerr, "A new framework for querying semantic networks," in *Proceedings of Museums and the Web 2012: the international conference for culture and heritage on-line*, 2012.
- [57] X. Glorot, A. Bordes, and Y. Bengio, "Deep sparse rectifier neural networks," in *AISTATS*, ser. JMLR Proceedings, vol. 15. JMLR.org, 2011, pp. 315–323.
- [58] K. He, X. Zhang, S. Ren, and J. Sun, "Deep residual learning for image recognition," in *CVPR*. IEEE Computer Society, 2016, pp. 770–778.
- [59] A. Shrikumar, P. Greenside, A. Shcherbina, and A. Kundaje, "Not just a black box: Learning important features through propagating activation differences," *CoRR*, vol. abs/1605.01713, 2016.
- [60] M. Ancona, E. Ceolini, C. Öztireli, and M. Gross, "Towards better understanding of gradient-based attribution methods for deep neural networks," in *ICLR (Poster)*. OpenReview.net, 2018.
- [61] G. Montavon, "Gradient-based vs. propagation-based explanations: An axiomatic comparison," in *Explainable AI*, ser. Lecture Notes in Computer Science. Springer, 2019, vol. 11700, pp. 253–265.
- [62] D. Balduzzi, M. Freaan, L. Leary, J. P. Lewis, K. W. Ma, and B. McWilliams, "The shattered gradients problem: If resnets are the answer, then what is the question?" in *ICML*, ser. Proceedings of Machine Learning Research, vol. 70. PMLR, 2017, pp. 342–350.
- [63] G. Montavon, A. Binder, S. Lapuschkin, W. Samek, and K.-R. Müller, "Layer-wise relevance propagation: An overview," in *Explainable AI*, ser. Lecture Notes in Computer Science. Springer, 2019, vol. 11700, pp. 193–209.
- [64] H. Zhang, J. Chen, H. Xue, and Q. Zhang, "Towards a unified evaluation of explanation methods without ground truth," *CoRR*, vol. abs/1911.09017, 2019.
- [65] S. Lapuschkin, A. Binder, K.-R. Müller, and W. Samek, "Understanding and comparing deep neural networks for age and gender classification," in *IEEE International Conference on Computer Vision Workshops*, 2017, pp. 1629–1638.
- [66] M. Everingham, L. Van Gool, C. K. I. Williams, J. Winn, and A. Zisserman, "The PASCAL Visual Object Classes Challenge 2007 (VOC2007) Results," <http://www.pascal-network.org/challenges/VOC/voc2007/workshop/index.html>.
- [67] R. Caruana, "Multitask learning," *Machine Learning*, vol. 28, no. 1, pp. 41–75, 1997.
- [68] M. Oquab, L. Bottou, I. Laptev, and J. Sivic, "Learning and transferring mid-level image representations using convolutional neural networks," in *CVPR*. IEEE Computer Society, 2014, pp. 1717–1724.
- [69] W. Zhang, R. Li, T. Zeng, Q. Sun, S. Kumar, J. Ye, and S. Ji, "Deep model based transfer and multi-task learning for biological image analysis," in *KDD*. ACM, 2015, pp. 1475–1484.
- [70] G. J. S. Litjens, T. Kooi, B. E. Bejnordi, A. A. A. Setio, F. Ciompi, M. Ghafoorian, J. A. W. M. van der Laak, B. van Ginneken, and C. I. Sánchez, "A survey on deep learning in medical image analysis," *Medical Image Analysis*, vol. 42, pp. 60–88, 2017.
- [71] Y. Gao and K. M. Mosalam, "Deep transfer learning for image-based structural damage recognition," *Comp.-Aided Civil and Infrastruct. Engineering*, vol. 33, no. 9, pp. 748–768, 2018.
- [72] L. Lenc and P. Král, "Unconstrained facial images: Database for face recognition under real-world conditions," in *MICAI (2)*, ser. Lecture Notes in Computer Science, vol. 9414. Springer, 2015, pp. 349–361.
- [73] G. B. Huang, M. Ramesh, T. Berg, and E. Learned-Miller, "Labeled faces in the wild: A database for studying face recognition in unconstrained environments," University of Massachusetts, Amherst, Tech. Rep. 07-49, October 2007.
- [74] M. Valleriani, "Prolegomena to the study of early modern commentators on Johannes de Sacrobosco's tractatus de sphaera," in *De sphaera of Johannes de Sacrobosco in the Early Modern Period: The Authors of the Commentaries*. Springer Nature, 2019, pp. 1–23.
- [75] Y. Sun, X. Wang, and X. Tang, "Deep learning face representation from predicting 10,000 classes," in *CVPR*. IEEE Computer Society, 2014, pp. 1891–1898.

- [76] F. Krätli and M. Valleriani, "CorpusTracer: A CIDOC database for tracing knowledge networks," *DSH*, vol. 33, no. 2, pp. 336–346, 2018.
- [77] S. Lang and B. Ommer, "Attesting similarity: Supporting the organization and study of art image collections with computer vision," *Digital Scholarship in the Humanities*, vol. 33, no. 4, pp. 845–856, 04 2018.
- [78] J. Bruna and S. Mallat, "Invariant scattering convolution networks," *IEEE Trans. Pattern Anal. Mach. Intell.*, vol. 35, no. 8, pp. 1872–1886, 2013.
- [79] S. Chmiela, H. E. Sauceda, K.-R. Müller, and A. Tkatchenko, "Towards exact molecular dynamics simulations with machine-learned force fields," *Nature Communications*, vol. 9, no. 1, Sep. 2018.
- [80] F. Anselmi, L. Rosasco, and T. Poggio, "On invariance and selectivity in representation learning," *Information and Inference*, vol. 5, no. 2, pp. 134–158, May 2016.
- [81] I. J. Goodfellow, Q. V. Le, A. M. Saxe, H. Lee, and A. Y. Ng, "Measuring invariances in deep networks," in *NIPS*. Curran Associates, Inc., 2009, pp. 646–654.
- [82] M. D. Rodriguez, J. Ahmed, and M. Shah, "Action MACH a spatio-temporal maximum average correlation height filter for action recognition," *2008 IEEE Conference on Computer Vision and Pattern Recognition*, pp. 1–8, 2008.
- [83] K. Soomro and A. Zamir, "Action recognition in realistic sports videos," *Advances in Computer Vision and Pattern Recognition*, vol. 71, pp. 181–208, 01 2014.
- [84] A. Dosovitskiy, P. Fischer, E. Ilg, P. Häusser, C. Hazirbas, V. Golkov, P. van der Smagt, D. Cremers, and T. Brox, "Flownet: Learning optical flow with convolutional networks," in *ICCV*. IEEE Computer Society, 2015, pp. 2758–2766.
- [85] M. Husson, "Remarks on two dimensional array tables in latin astronomy: a case study in layout transmission," *Suhayl. Journal for the History of the Exact and Natural Sciences in Islamic Civilisation*, vol. 13, pp. 103–117, 2014.
- [86] S. Schreiber, S. Agne, I. Wolf, A. Dengel, and S. Ahmed, "Deep-DeSRT: Deep learning for detection and structure recognition of tables in document images," in *ICDAR*. IEEE, 2017, pp. 1162–1167.

Building and Interpreting Deep Similarity Models

(SUPPLEMENTARY MATERIAL)

Oliver Eberle, Jochen Büttner, Florian Kräutli, Klaus-Robert Müller, Matteo Valleriani, Grégoire Montavon

In this Supplement, we give proofs and derivations for the ‘Hessian×Product’ baseline and for our proposed BiLRP method. We also give details on the procedure we use in the paper to render BiLRP explanations on image data.

APPENDIX A

‘HESSIAN×PRODUCT’ BASELINE

The ‘Hessian×Product’ (HP) baseline we consider in this paper applies to similarity models of the type:

$$y(\mathbf{x}, \mathbf{x}') = \langle \phi(\mathbf{x}), \phi(\mathbf{x}') \rangle$$

a dot product on a feature map $\phi: \mathbb{R}^d \rightarrow \mathbb{R}^h$ satisfying first-order positive homogeneity i.e. $\forall \mathbf{x}, \forall t>0: \phi(t\mathbf{x}) = t\phi(\mathbf{x})$.

A.1 Derivation of HP

We derive Hessian×Product as the result of a Taylor expansion of the similarity model at the root point $(\tilde{\mathbf{x}}, \tilde{\mathbf{x}}') = (\varepsilon\mathbf{x}, \varepsilon\mathbf{x}')$ with ε almost zero. For the zero-order term, we get:

$$y(\tilde{\mathbf{x}}, \tilde{\mathbf{x}}') = 0$$

Let ∇ and ∇' be the gradient operators with respect to the features forming \mathbf{x} and \mathbf{x}' respectively. First-order terms associated to the features of \mathbf{x} are given by:

$$\begin{aligned} R_i &= [\nabla y(\tilde{\mathbf{x}}, \tilde{\mathbf{x}}')]_i \cdot (x_i - \tilde{x}_i) \\ &= [\nabla \sum_m \phi_m(\tilde{\mathbf{x}}) \phi_m(\tilde{\mathbf{x}}')]_i \cdot x_i \\ &= [\sum_m (\nabla \phi_m(\tilde{\mathbf{x}})) \cdot \phi_m(\tilde{\mathbf{x}}')]_i \cdot x_i \\ &= [\sum_m (\nabla \phi_m(\tilde{\mathbf{x}})) \cdot \phi_m(\mathbf{0})]_i \cdot x_i \\ &= 0 \end{aligned}$$

In a similar way, for the features of \mathbf{x}' , we get $R_{i'} = 0$. To extract the interaction terms $R_{ii'}$, we first show that $\forall t>0: \nabla \phi_m(t\mathbf{x}) = \nabla \phi_m(\mathbf{x})$:

$$\nabla \phi_m(t\mathbf{x}) = t^{-1} \frac{\partial}{\partial \mathbf{x}} \phi_m(t\mathbf{x}) = t^{-1} \frac{\partial}{\partial \mathbf{x}} t\phi_m(\mathbf{x}) = \nabla \phi_m(\mathbf{x})$$

Then, we develop the interaction terms of the Taylor expansion as:

$$\begin{aligned} R_{ii'} &= [\nabla^2 y(\tilde{\mathbf{x}}, \tilde{\mathbf{x}}')]_{ii'} \cdot (x_i - \tilde{x}_i) \cdot (x'_{i'} - \tilde{x}'_{i'}) \\ &= [\sum_m \nabla^2 \phi_m(\tilde{\mathbf{x}}) \phi_m(\tilde{\mathbf{x}}')]_{ii'} \cdot x_i x'_{i'} \\ &= [\sum_m \nabla \nabla' \phi_m(\tilde{\mathbf{x}}) \phi_m(\tilde{\mathbf{x}}')]_{ii'} \cdot x_i x'_{i'} \\ &= [\sum_m (\nabla \phi_m(\tilde{\mathbf{x}})) \otimes (\nabla' \phi_m(\tilde{\mathbf{x}}'))]_{ii'} \cdot x_i x'_{i'} \end{aligned}$$

where \otimes denotes the outer product, we apply the property shown above ($\nabla \phi_m(t\mathbf{x}) = \nabla \phi_m(\mathbf{x})$) to get

$$= [\sum_m (\nabla \phi_m(\mathbf{x})) \otimes (\nabla' \phi_m(\mathbf{x}'))]_{ii'} \cdot x_i x'_{i'} \quad (1)$$

and finally, we apply the steps in reverse order

$$\begin{aligned} &= [\sum_m \nabla \nabla' \phi_m(\mathbf{x}) \phi_m(\mathbf{x}')]_{ii'} \cdot x_i x'_{i'} \\ &= [\sum_m \nabla^2 \phi_m(\mathbf{x}) \phi_m(\mathbf{x}')]_{ii'} \cdot x_i x'_{i'} \\ &= [\nabla^2 y(\mathbf{x}, \mathbf{x}')]_{ii'} \cdot x_i x'_{i'}. \end{aligned}$$

The last line corresponds to the HP baseline.

A.2 Conservation of HP

We show that ‘Hessian×Product’ sums to the similarity score, and thus constitutes an explanation that is conservative. For this, we can first show that $\mathbf{x}^\top \nabla \phi_m(\mathbf{x}) = \phi_m(\mathbf{x})$:

$$\mathbf{x}^\top \nabla \phi_m(t\mathbf{x}) = \frac{\partial}{\partial t} \phi_m(t\mathbf{x}) = \frac{\partial}{\partial t} t\phi_m(\mathbf{x}) = \phi_m(\mathbf{x})$$

Choosing $t = 1$ completes the proof. (This result is known as Euler’s homogeneous function theorem.)

Starting from Eq. (1), we then write:

$$\begin{aligned} \sum_{ii'} R_{ii'} &= \sum_{ii'} [\sum_m (\nabla \phi_m(\mathbf{x})) \otimes (\nabla' \phi_m(\mathbf{x}'))]_{ii'} \cdot x_i x'_{i'} \\ &= \sum_m \sum_i x_i [\nabla \phi_m(\mathbf{x})]_i \cdot \sum_{i'} x'_{i'} [\nabla' \phi_m(\mathbf{x}')]_{i'} \\ &= \sum_m \mathbf{x}^\top \nabla \phi_m(\mathbf{x}) \cdot \mathbf{x}'^\top \nabla' \phi_m(\mathbf{x}') \\ &= \sum_m \phi_m(\mathbf{x}) \cdot \phi_m(\mathbf{x}') \\ &= y(\mathbf{x}, \mathbf{x}') \end{aligned}$$

which shows that the explanation is conservative.

A.3 ‘Gradient×Input’ Formulation of HP

We show that ‘Hessian×Product’ can be rewritten as $2 \times h$ ‘Gradient×Input’ (GI) computations. Starting from Eq. (1), we get:

$$\begin{aligned} R_{ii'} &= [\sum_m (\nabla \phi_m(\mathbf{x})) \otimes (\nabla' \phi_m(\mathbf{x}'))]_{ii'} \cdot x_i x'_{i'} \\ &= [\sum_m (\nabla \phi_m(\mathbf{x}) \odot \mathbf{x}) \otimes (\nabla' \phi_m(\mathbf{x}') \odot \mathbf{x}')]_{ii'} \\ &= [\sum_m \text{GI}(\phi_m, \mathbf{x}) \otimes \text{GI}(\phi_m, \mathbf{x}')]_{ii'} \end{aligned}$$

Therefore, scores $R_{ii'}$ produced by HP are the elements of a sum of outer products of GI computations.

APPENDIX B

DERIVATION OF BiLRP

The deep Taylor decomposition [1] (DTD) framework we use to derive BiLRP propagation rules assumes that relevance propagated up to a certain layer can be modeled as

$$\hat{R}_{kk'}(\mathbf{a}) = a_k a_{k'} c_{kk'}$$

i.e. a product of activations in the two branches of the similarity computation, multiplied by a term $c_{kk'}$ assumed

to be constant and set in a way that $\widehat{R}_{kk'}(\mathbf{a}) = R_{kk'}$. DTD seeks to propagate the modeled relevance to the layer below by identifying the terms of a Taylor expansion. In the following, we distinguish between (1) linear/ReLU layers, and (2) positively homogeneous layers (e.g. min- or max-pooling).

B.1 Linear/ReLU Layers

These layers produce output activations of the type

$$\begin{aligned} a_k &= (\sum_j a_j w_{jk})^+ \\ a_{k'} &= (\sum_{j'} a_{j'} w_{j'k'})^+ \end{aligned}$$

where the weighted sum can be either a dense layer, or a convolution. The relevance model can be written as:

$$\begin{aligned} \widehat{R}_{kk'}(\mathbf{a}) &= a_k a_{k'} c_{kk'} \\ &= (\sum_j a_j w_{jk})^+ (\sum_{j'} a_{j'} w_{j'k'})^+ c_{kk'} \end{aligned}$$

When neurons a_k and $a_{k'}$ are jointly activated (i.e. $a_k, a_{k'} > 0$), a second-order Taylor expansion of $R_{kk'}$ at some reference point $\tilde{\mathbf{a}}$ is given by:

$$\begin{aligned} \widehat{R}_{kk'}(\mathbf{a}) &= (\sum_j \tilde{a}_j w_{jk}) (\sum_{j'} \tilde{a}_{j'} w_{j'k'}) c_{kk'} \\ &+ \sum_j (a_j - \tilde{a}_j) w_{jk} (\sum_{j'} \tilde{a}_{j'} w_{j'k'}) c_{kk'} \\ &+ \sum_{j'} (\sum_j \tilde{a}_j w_{jk}) (a_{j'} - \tilde{a}_{j'}) w_{j'k'} c_{kk'} \\ &+ \sum_{jj'} (a_j - \tilde{a}_j) w_{jk} (a_{j'} - \tilde{a}_{j'}) w_{j'k'} c_{kk'} \end{aligned}$$

BiLRP chooses the reference point $\tilde{\mathbf{a}}$ to be subject to the following two constraints:

- 1) very close to the ReLU hinges of neurons k and k' (but still on the activated domain)
- 2) on the plane $\{\tilde{\mathbf{a}}(t, t') \mid t, t' \in \mathbb{R}\}$ where

$$\begin{aligned} [\tilde{\mathbf{a}}(t, t')]_j &= a_j - t a_j \cdot (1 + \gamma \cdot 1_{w_{jk} > 0}) \\ [\tilde{\mathbf{a}}(t, t')]_{j'} &= a_{j'} - t' a_{j'} \cdot (1 + \gamma \cdot 1_{w_{j'k'} > 0}) \end{aligned}$$

with γ a hyperparameter.

We now analyze the different terms of the expansion at this reference point.

- The zero-order term is zero.
- The first-order terms are also zero because the reference point is chosen at the *intersection* of the ReLU hinges of neurons k and k' , hence the non-differentiated term is zero.
- The interaction terms are given by:

$$\begin{aligned} R_{jj' \leftarrow kk'} &= t a_j (1 + \gamma 1_{w_{jk} > 0}) \\ &\quad \cdot t' a_{j'} (1 + \gamma 1_{w_{j'k'} > 0}) \\ &\quad \cdot w_{jk} w_{j'k'} c_{kk'} \\ &= t t' a_j a_{j'} \rho(w_{jk}) \rho(w_{j'k'}) c_{kk'} \end{aligned}$$

where $\rho(w_{jk}) = w_{jk} + \gamma w_{jk}^+$ and where the product of parameters tt' must still be resolved.

Because we expand a bilinear form, and because zero-order and first-order terms are zero, the constraint $\sum_{jj'} R_{jj' \leftarrow kk'} = R_{kk'}$ must be satisfied. This constraint

allows us to resolve the product tt' , leading to the following closed-form expression for the interaction terms:

$$R_{jj' \leftarrow kk'} = \frac{a_j a_{j'} \rho(w_{jk}) \rho(w_{j'k'})}{\sum_{jj'} a_j a_{j'} \rho(w_{jk}) \rho(w_{j'k'})} R_{kk'}$$

This propagation rule is also consistent with the case where a_k or $a_{k'}$ are zero and where no relevance needs to be redistributed. Aggregate relevance scores for the layer below are obtained by summing over neurons in the higher-layer:

$$\begin{aligned} R_{jj'} &= \sum_{kk'} R_{jj' \leftarrow kk'} \\ &= \sum_{kk'} \frac{a_j a_{j'} \rho(w_{jk}) \rho(w_{j'k'})}{\sum_{jj'} a_j a_{j'} \rho(w_{jk}) \rho(w_{j'k'})} R_{kk'} \end{aligned} \quad (2)$$

This last equation is the propagation rule used by BiLRP to propagate relevance in linear/ReLU layers.

B.2 Positively Homogeneous Layers

When a_k and $a_{k'}$ are positively homogeneous functions of their input activations (e.g. min- and max-pooling layers), the relevance model can be expressed in terms of the Hessian:

$$\begin{aligned} \widehat{R}_{kk'}(\mathbf{a}) &= a_k a_{k'} c_{kk'} \\ &= (\sum_j a_j [\nabla a_k]_j) (\sum_{j'} a_{j'} [\nabla a_{k'}]_{j'}) c_{kk'} \\ &= \sum_{jj'} a_j a_{j'} [\nabla^2 a_k a_{k'}]_{jj'} c_{kk'} \end{aligned}$$

The last form can also be interpreted as the interaction terms of a Taylor expansion of $\widehat{R}_{kk'}$ at $\tilde{\mathbf{a}} = \varepsilon \mathbf{a}$ with ε almost zero. Zero-order and first-order terms of the expansion vanish, and interaction terms can be rewritten in a propagation-like manner as:

$$R_{jj' \leftarrow kk'} = \frac{a_j a_{j'} [\nabla^2 a_k a_{k'}]_{jj'}}{\sum_{jj'} a_j a_{j'} [\nabla^2 a_k a_{k'}]_{jj'}} R_{kk'},$$

and finally,

$$R_{jj'} = \sum_{kk'} \frac{a_j a_{j'} [\nabla^2 a_k a_{k'}]_{jj'}}{\sum_{jj'} a_j a_{j'} [\nabla^2 a_k a_{k'}]_{jj'}} R_{kk'}, \quad (3)$$

which is the BiLRP propagation rule we use in these layers.

APPENDIX C

FACTORIZATION OF BiLRP

In this appendix, we show how the propagation rules in Equations (2) and (3) can be factorized to be expressed as compositions of standard LRP [2] propagation rules. In the top layer, the dot product similarity can be written as:

$$y = \sum_{kk'} a_k a_{k'} 1_{\text{id}(k)=\text{id}(k')}$$

where 'id' is a function returning the neuron index in its respective branch (a number from 1 to h). Relevance scores can be identified and developed as:

$$\begin{aligned} R_{kk'} &= a_k a_{k'} 1_{\text{id}(k)=\text{id}(k')} \\ &= a_k a_{k'} \sum_{m=1}^h 1_{\text{id}(k)=m} 1_{\text{id}(k')=m} \\ &= \sum_{m=1}^h \underbrace{a_k 1_{\text{id}(k)=m}}_{R_{km}} \cdot \underbrace{a_{k'} 1_{\text{id}(k')=m}}_{R_{k'm}} \end{aligned}$$

where we have extracted the desired factor structure. We now apply an inductive argument: Assume that at some layer, $R_{kk'}$ factorizes as $R_{kk'} = \sum_{m=1}^h R_{km} R_{k'm}$. We can show that the same holds in the layer below, in particular, Eq. (2) can be rewritten as:

$$\begin{aligned} R_{jj'} &= \sum_{kk'} \frac{a_j a_{j'} \rho(w_{jk}) \rho(w_{j'k'})}{\sum_{jj'} a_j a_{j'} \rho(w_{jk}) \rho(w_{j'k'})} \sum_{m=1}^h R_{km} R_{k'm} \\ &= \sum_{m=1}^h \sum_{kk'} \frac{a_j \rho(w_{jk}) a_{j'} \rho(w_{j'k'})}{\sum_j a_j \rho(w_{jk}) \sum_{j'} a_{j'} \rho(w_{j'k'})} R_{km} R_{k'm} \\ &= \sum_{m=1}^h \left(\underbrace{\sum_k \frac{a_j \rho(w_{jk})}{\sum_j a_j \rho(w_{jk})} R_{km}}_{R_{jm}} \right) \cdot \left(\underbrace{\sum_{k'} \frac{a_{j'} \rho(w_{j'k'})}{\sum_{j'} a_{j'} \rho(w_{j'k'})} R_{k'm}}_{R_{j'm}} \right) \end{aligned}$$

where we identify a similar factorization. Furthermore, terms of the factorization can be computed using standard LRP rules, here, LRP- γ [3]. Similarly, Eq. (3) can be rewritten as:

$$\begin{aligned} R_{jj'} &= \sum_{kk'} \frac{a_j a_{j'} [\nabla^2 a_k a_{k'}]_{jj'}}{\sum_{jj'} a_j a_{j'} [\nabla^2 a_k a_{k'}]_{jj'}} \sum_{m=1}^h R_{km} R_{k'm} \\ &= \sum_{m=1}^h \sum_{kk'} \frac{a_j [\nabla a_k]_j a_{j'} [\nabla a_{k'}]_{j'}}{\sum_j a_j [\nabla a_k]_j \sum_{j'} a_{j'} [\nabla a_{k'}]_{j'}} R_{km} R_{k'm} \\ &= \sum_{m=1}^h \left(\underbrace{\sum_k \frac{a_j [\nabla a_k]_j}{\sum_j a_j [\nabla a_k]_j} R_{km}}_{R_{jm}} \right) \cdot \left(\underbrace{\sum_{k'} \frac{a_{j'} [\nabla a_{k'}]_{j'}}{\sum_{j'} a_{j'} [\nabla a_{k'}]_{j'}} R_{k'm}}_{R_{j'm}} \right) \end{aligned}$$

which again factorizes into a composition of LRP-type propagation rules.

APPENDIX D THEORETICAL PROPERTIES OF BiLRP

In this appendix, we give proofs for the theoretical properties stated in Section 3.3 of the paper.

D.1 Conservation of BiLRP

An important property of LRP [2] is conservation, i.e. the relevance scores assigned to the input features sum to the prediction output¹. Similar results can be obtained for BiLRP.

Proposition 1. *For deep rectifier networks with zero biases, BiLRP is conservative, i.e. $\sum_{ii'} R_{ii'} = y(\mathbf{x}, \mathbf{x}')$.*

We first show conservation when propagating with Eq. (2) in a linear/ReLU layer:

$$\begin{aligned} \sum_{jj'} R_{jj'} &= \sum_{jj'} \sum_{kk'} \frac{a_j a_{j'} \rho(w_{jk}) \rho(w_{j'k'})}{\sum_{jj'} a_j a_{j'} \rho(w_{jk}) \rho(w_{j'k'})} R_{kk'} \\ &= \sum_{kk'} \frac{\sum_{jj'} a_j a_{j'} \rho(w_{jk}) \rho(w_{j'k'})}{\sum_{jj'} a_j a_{j'} \rho(w_{jk}) \rho(w_{j'k'})} R_{kk'} = \sum_{kk'} R_{kk'} \end{aligned}$$

1. In LRP, exact conservation requires using non-dissipative propagation rules (e.g. LRP-0 and LRP- γ), as well as avoiding contribution of biases (e.g. by training a model with biases set to zero).

Same conservation property can be shown for the propagation rule in Eq. (3). Because these rules are applied repeatedly at each layer, we get the chain of equalities

$$\sum_{ii'} R_{ii'} = \dots = \sum_{jj'} R_{jj'} = \sum_{kk'} R_{kk'} = \dots = y(\mathbf{x}, \mathbf{x}')$$

where we observe that conservation also holds globally.

D.2 HP as a Special Case of BiLRP

A result due to [4] is that application of a special case of LRP (referred by [3] as LRP-0, or LRP- γ with $\gamma = 0$) at each layer of the network produces an explanation that is equivalent to Gradient \times Input. A similar result can be shown for BiLRP.

Proposition 2. *When $\gamma = 0$, explanations produced by BiLRP reduce to those of Hessian \times Product.*

Rewriting relevance scores as $R_{jj'} = a_j a_{j'} c_{jj'}$ and $R_{kk'} = a_k a_{k'} c_{kk'}$ and observing that for $\gamma = 0$, we have $\rho(w_{jk}) = w_{jk}$, the propagation from one layer to another can be written for Eq. (2) as:

$$\begin{aligned} c_{jj'} &= \sum_{kk'} w_{jk} w_{j'k'} \frac{a_k}{\sum_j a_j w_{jk}} \frac{a_{k'}}{\sum_{j'} a_{j'} w_{j'k'}} c_{kk'} \\ &= \sum_{kk'} w_{jk} w_{j'k'} \mathbf{1}_{a_k > 0} \mathbf{1}_{a_{k'} > 0} c_{kk'} \\ &= \sum_{kk'} [\nabla a_k]_j [\nabla a_{k'}]_{j'} c_{kk'} \end{aligned}$$

and similarly for Eq. (3) as:

$$\begin{aligned} c_{jj'} &= \sum_{kk'} [\nabla^2 a_k a_{k'}]_{jj'} c_{kk'} \\ &= \sum_{kk'} [\nabla a_k]_j [\nabla a_{k'}]_{j'} c_{kk'} \end{aligned}$$

For the considered class of functions, this relation is equivalent to the formula for propagating second-order derivatives (cf. [5]), where $c_{jj'}$ and $c_{kk'}$ denote $[\nabla^2 y]_{jj'}$ and $[\nabla^2 y]_{kk'}$ respectively. Hence, we get at the end of the LRP procedure the quantity $c_{ii'} = [\nabla^2 y]_{ii'}$ and therefore $R_{ii'} = x_i x'_{i'} c_{ii'}$ is equivalent to ‘Hessian \times Product’.

D.3 Product Approximation in BiLRP

We highlight in the following the product structure of relevance scores produced by BiLRP at each layer. This product structure supports the relevance model used by DTD, from which BiLRP propagation rules can be derived.

Proposition 3. *The relevance computed by BiLRP at each layer can be rewritten as $R_{jj'} = a_j a_{j'} c_{jj'}$, where $c_{jj'}$ is locally approximately constant.*

In the top layer, we have $c_{kk'} = \mathbf{1}_{\text{id}(k)=\text{id}(k')}$ (cf. Appendix C), which is constant. We apply an inductive argument: Assume that at some layer, $c_{kk'}$ is locally approximately constant, we would like to show that the same holds for $c_{jj'}$ in the layer below.

Relevance scores in Eq. (2) can be rewritten as $R_{jj'} = a_j a_{j'} c_{jj'}$ with:

$$c_{jj'} = \sum_{kk'} \rho(w_{jk}) \rho(w_{j'k'}) \frac{(\sum_j a_j w_{jk})^+ (\sum_{j'} a_{j'} w_{j'k'})^+}{\sum_{jj'} a_j a_{j'} \rho(w_{jk}) \rho(w_{j'k'})} c_{kk'}$$

The term $c_{jj'}$ depends on a_j and $a_{j'}$ only through (1) nested sums, which can be seen as diluting the effect of these activations, and (2) the term $c_{kk'}$ which we have assumed as a starting point to be locally approximately constant.

Similarly, for Eq. (3), the redistributed relevance can be written in product form, with $c_{jj'} = \sum_{kk'} [\nabla^2 a_k a_{k'}]_{jj'} c_{kk'}$. This time, $c_{jj'}$ depends on local activations through (1) a combination of a nested sum and a second-order differentiation, with the same diluting effect as above, and (2) the term $c_{kk'}$ which is locally approximately constant.

Overall, in both cases, the weak dependency of $c_{jj'}$ on local activations provides support for treating this term as constant in the relevance model used by DTD.

APPENDIX E COARSE-GRAINED EXPLANATIONS

When the input has d dimensions, BiLRP explanations have size d^2 , which can be very large. In practice, similarity does not necessarily need to be attributed to every single pair of pixels or input dimensions. A coarse-grained explanation in terms of groups of features jointly representing a super-pixel, a character, or a word, is often sufficient. Let $(\mathcal{I}_1, \mathcal{I}_2, \dots)$ and $(\mathcal{I}'_1, \mathcal{I}'_2, \dots)$ be two partitions of features for the two input examples x and x' . These partitions form the coarse-grained structure in terms of which we would like to produce an explanation. Coarse-grained relevance scores are then given by:

$$R_{\mathcal{I}\mathcal{I}'} = \sum_{i \in \mathcal{I}} \sum_{i' \in \mathcal{I}'} R_{ii'}.$$

When the original explanation is conservative, it can be verified that the same holds for the coarse-grained explanation ($\sum_{\mathcal{I}\mathcal{I}'} R_{\mathcal{I}\mathcal{I}'} = \sum_{\mathcal{I}\mathcal{I}'} \sum_{ii' \in \mathcal{I}\mathcal{I}'} R_{ii'} = \sum_{ii'} R_{ii'}$).

APPENDIX F RENDERING OF BiLRP EXPLANATIONS

BiLRP explanations of images are composed of ($\#$ pixels \times $\#$ pixels) scores connecting pairs of pixels in the two input images. Visually rendering these high-dimensional explanations requires to compress them while retaining the relevant information they contain. The rendering procedure we use in this paper is given in Algorithm 1.

Algorithm 1 Rendering of BiLRP explanations

```

 $R_{\mathcal{I}\mathcal{I}'} \leftarrow \sum_{i \in \mathcal{I}} \sum_{i' \in \mathcal{I}'} R_{ii'}$            (coarse-graining)
 $R_{\mathcal{I}\mathcal{I}'} \leftarrow R_{\mathcal{I}\mathcal{I}'} / \sqrt[4]{\mathbb{E}[R_{\mathcal{I}\mathcal{I}'}^4]}$        (normalization)
 $R_{\mathcal{I}\mathcal{I}'} \leftarrow R_{\mathcal{I}\mathcal{I}'} - \text{clip}(R_{\mathcal{I}\mathcal{I}'}, [-l, l])$    (sparsification)
 $\Delta = h - l$ 
 $R_{\mathcal{I}\mathcal{I}'} \leftarrow \text{clip}(R_{\mathcal{I}\mathcal{I}'}, [-\Delta, \Delta]) / \Delta$  (thresholding)
for all  $R_{\mathcal{I}\mathcal{I}'} \neq 0$  do
   $\alpha = |R_{\mathcal{I}\mathcal{I}'}|^p$                                (set opacity)
  if  $R_{\mathcal{I}\mathcal{I}'} > 0$  then
    connect( $\mathcal{I}, \mathcal{I}'$ , red,  $\alpha$ )
  else
    connect( $\mathcal{I}, \mathcal{I}'$ , blue,  $\alpha$ )
  end if
end for

```

The procedure pools relevance scores on super-pixels, normalizes them, shrinks them so that only a limited number of connections need to be plotted, thresholds them so that they fit into a finite color space, and raises them to some power p . The parameter l controls the level of sparsification and we tune it mostly for computational reasons. The parameter h forces all scores beyond a certain range to be plotted to the maximum color value. The parameter p lets the explanation focus on all or the highest relevance scores. A large value for p makes it more easily interpretable, however contributions to similarity that are spread to a larger group of input features can become visually imperceptible. Example of heatmaps with different values of p are shown in Fig. 1. Parameters retained for each dataset, as well as pooling and input sizes are given in Table 1.

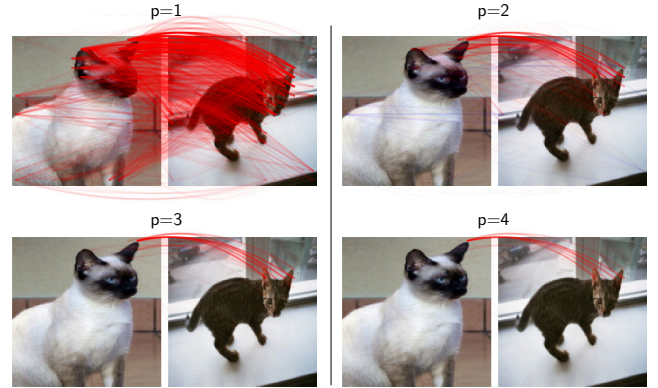


Fig. 1: Effect of the parameter p on the rendering of the explanation. The higher the parameter p , the sparser the explanation.

TABLE 1: Parameters used on each dataset for rendering BiLRP explanations.

Dataset	input size	pool	l	h	p
Pascal VOC 2007	128×128	8×8	0.25	13	2
Faces (UFI & LFW)	64×64	4×4	0.3	60	1
UCF Sport	128×128	8×8	0.25	20	1
Sphaera (illustrations)	96×96	6×6	0.25	15	2
Sphaera (tables)	140×140	20×20	0.01	4	2

REFERENCES

- [1] G. Montavon, S. Lapuschkin, A. Binder, W. Samek, and K.-R. Müller, “Explaining nonlinear classification decisions with deep Taylor decomposition,” *Pattern Recognition*, vol. 65, pp. 211–222, 2017.
- [2] S. Bach, A. Binder, G. Montavon, F. Klauschen, K.-R. Müller, and W. Samek, “On pixel-wise explanations for non-linear classifier decisions by layer-wise relevance propagation,” *PLoS ONE*, vol. 10, no. 7, p. e0130140, 07 2015.
- [3] G. Montavon, A. Binder, S. Lapuschkin, W. Samek, and K.-R. Müller, “Layer-wise relevance propagation: An overview,” in *Explainable AI*, ser. Lecture Notes in Computer Science. Springer, 2019, vol. 11700, pp. 193–209.
- [4] A. Shrikumar, P. Greenside, A. Shcherbina, and A. Kundaje, “Not just a black box: Learning important features through propagating activation differences,” *CoRR*, vol. abs/1605.01713, 2016.
- [5] Y. LeCun, L. Bottou, G. B. Orr, and K.-R. Müller, “Efficient back-prop,” in *Neural Networks: Tricks of the Trade (2nd ed.)*, ser. Lecture Notes in Computer Science. Springer, 2012, vol. 7700, pp. 9–48.